Mechanical and Transport Properties of the Poly(ethylene oxide)−Poly(acrylic acid) Double Network Hydrogel from Molecular Dynamic Simulations

Seung Soon Jang and William A. Goddard, III*

Materials and Process Simulation Center (MC 139-74), California Institute of Technology, Pasadena, California 91125

M. Yashar S. Kalani

Howard Hughes Medical Institute & Stanford University Institute of Regenerative Medicine & Stem Cell Biology and the Department of Neurosurgery, Stanford, California 94305

Received: August 30, 2006; In Final Form: December 8, 2006

We used atomistic molecular dynamics (MD) simulations to investigate the mechanical and transport properties of the PEO−PAA double network (DN) hydrogel with 76 wt % water content. By analyzing the pair correlation functions for polymer−water pairs and for ion−water pairs and the solvent accessible surface area, we found that the solvation of polymer and ion in the DN hydrogel is enhanced in comparison with both PEO and PAA single network (SN) hydrogels. The effective mesh size of this DN hydrogel is smaller than that of the SN hydrogels with the same water content and the same molecular weight between the cross-linking points (M_c). Applying uniaxial extensions, we obtained the stress−strain curves for the hydrogels. This shows that the DN hydrogel has a sudden increase of stress above ∼100% strain, much higher than the sum of the stresses of the two SN hydrogels at the same strain. This arises because PEO has a smaller M_c value than PAA, so that the PEO in the DN reaches fully stretched out at 100% strain that corresponds to 260% strain in the PEO SN (beyond this point, the bond stretching and the angle bending increase dramatically). We also calculated the diffusion coefficients of solutes such as D-glucose and ascorbic acid in the hydrogels, where we find that the diffusion coefficients of those solutes in the DN hydrogel are 60% of that in the PEO SN and 40% of that in the PAA SN due to its smaller effective mesh size.

1. Introduction

A hydrogel is a three-dimensionally cross-linked hydrophilic polymer network that may absorb and retain a large amount of water, up to thousands of times its dry weight.[1] The excellent biocompatibility and smart stimulus−response properties of hydrogels make them most promising for such applications as tissue engineering and drug delivery.[2−7] Recently, these efforts have accelerated tremendously with rapid progress in synthesis technology realizing exactly defined molecular architectures, which promise to provide better medical treatment and health care.

Among the artificial materials for such hydrogel technology, we are interested in poly(ethylene oxide) (PEO) (Figure 1a) and poly(acrylic acid) (PAA) (Figure 1b) due to their relatively low toxicity as well as good hydrophilicity[4,7] which show promise for tissue regeneration and controlled drug release. However, their mechanical fragility in their individual single network (SN) hydrogel has impeded applications to replacement or augmentation of the injured tissue consisting of extracellular matrix (ECM), which requires high mechanical strength.

In this situation, the formation of interpenetrating but independently cross-linked double network (DN) hydrogels has been suggested as a strategy to achieve the high mechanical strength required for the purpose of tissue replacement.[8−14] In general, a DN hydrogel consists of two polymeric networks: one is made of highly cross-linked polymers, and the other is made of loosely cross-linked polymers. Gong and co-workers reported excellent mechanical performance for DN hydrogels consisting of poly(2-acrylamide-2-methyl-propane sulfonic acid) and poly(acrylamide). They found that the fracture stress of this DN hydrogel is ∼20 times larger than those of individual SN hydrogels.[8,13,14]

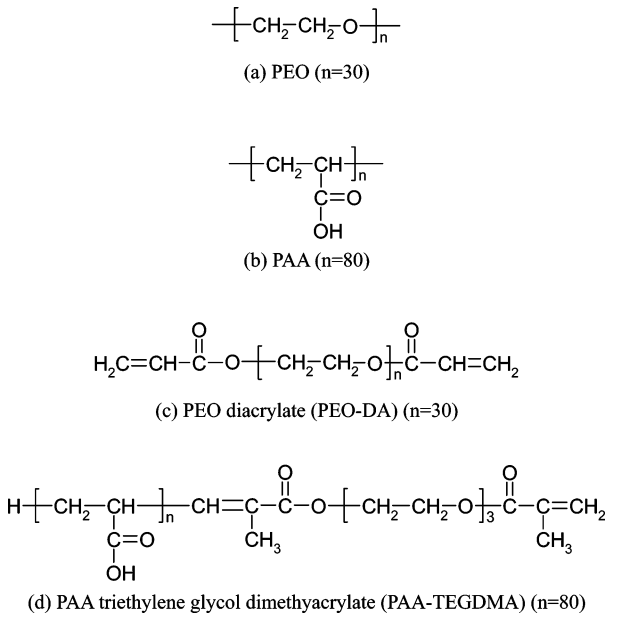

Figure 1. Chemical structures of PEO, PAA, and their macromers for three-dimensional network formation.

Recently, Frank and his co-workers have reported their studies[9−11] on the DN hydrogel consisting of poly(ethylene

10.1021/jp0656330 CCC: $37.00
Published on Web 01/24/2007

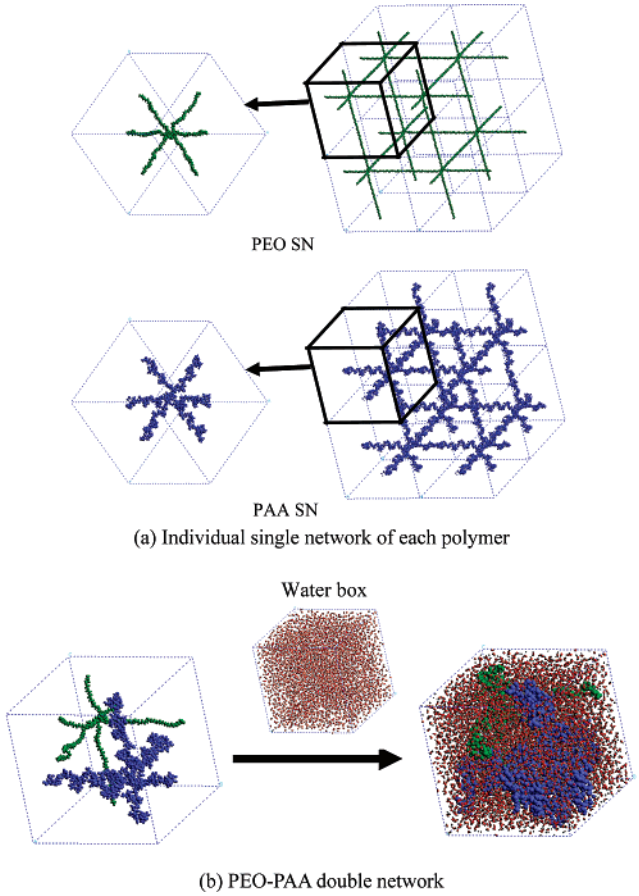

Figure 2. Illustration of the construction of the single networks and the double network of PEO and PAA.

oxide) (PEO) and poly(acrylic acid) (PAA) for the purpose of corneal applications, also showing an excellent mechanical property and biocompatibility.

A noteworthy point is that in order to maximize the mechanical strength of DN hydrogel, one component network should have a higher cross-linking density while another one should have a lower cross-linking density.[8,12−14] On the basis of experimental observations, an explanation for this asymmetric cross-linking has been suggested as follows: if both of the two respective networks have high cross-linking, the DN hydrogel becomes too brittle; however, if both networks have low cross-linking, then the elastic modulus of the DN hydrogel is as poor as just their individual components. This explanation seems to assume that, through such asymmetric cross-linking, the loosely cross-linked network allows some room for conformational relaxation at small strain but restricts a large extent of deformation topologically even though it has not been thoroughly investigated at the molecular level.

An important property for some applications of these materials is the transport of small solute molecules such as glucose and vitamins that are essential for the vitality of living organs. From numerous studies[15−21] on this topic, a general consensus is that the diffusion of these molecules depends on molecular variables such as the size of the solute, degree of cross-linking of the hydrogel, and molecular interaction of the solute with the polymer chain of hydrogel as well as some environmental variables such as the pH, temperature, and electric field. Thus, it is quite desirable to achieve good transport properties in the DN hydrogel through the structure−properties relationships of hydrogel established investigating molecular and environmental variables.

In this context, molecular modeling using molecular dynamics (MD) and Monte Carlo (MC) simulations can provide valuable information about how the structural and transport properties of DN hydrogel depend on structural variables. The statistical mechanical aspects of the SN were introduced in the early 1940s,[22−26] and MD simulations focusing on water in SN hydrogels,[27−31] no theoretically investigated have yet been reported for DN hydrogels.

This paper presents MD studies on the mechanical and transport properties of the PEO−PAA DN hydrogel. A primary objective is to characterize the structural change of this PEO−PAA DN hydrogel during its deformation process in comparison with those of individual SN hydrogels such as PEO and PAA SN hydrogels. This comparison provides an understanding of the superior mechanical strength of DN hydrogel. A second objective is to investigate the diffusion of small solute molecules including water. Because of the abundance of water in hydrogel, all of the components in hydrogel are solvated at some concentration. We expect that these atomistic MD simulations including explicit water molecules will provide a useful description of the solute mobility by calculating the explicit interaction between the solute and water molecules.

2. Simulations Details

2.1. Force Field and MD Parameters. In this study, we used the generic DREIDING force field[32] that has been successfully used for studies on various systems such as the hydrated polymer electrolyte membranes,[33,34] the surfactant-mediated air−water interface,[35,36] and the self-assemblies of organic molecules.[37−39]

TABLE 1: Characteristics of Hydrogels from 1.2 ns of MD Simulations

	PEO SN	PAA SN	PEO−PAA DN
density at 300 K (g/cm^3)	1.026 ± 0.006	1.160 ± 0.004	1.136 ± 0.003
simulated cell size (Å)	30.27 ± 0.07	52.85 ± 0.08	55.70 ± 0.10
number of water molecules	782	4218	5000
(water content wt %)	(76)	(76)	(76)
molecular weight of macromer (M_c)	1446	NA	1446
(degree of polymerization)	(30)		(30)
PEO−DA			
PAA−TEGDMA	NA	7804	7804
		(80)	(80)
molecular weight ratio (MW_{PEO}:MW_{PAA})	1:0	0:1	1:5.4
volume fraction of polymer in swollen state, $v_{2,s}$	0.1228	0.1844	0.1764
characteristic ratio (C_n)	4.0[a]	6.7[b]	NA
segmental length (l) (Å)	3.736	2.687	NA
mesh size (ξ) (Å, theory, eq 3)	149.26	220.36	NA
mesh size (ξ) (Å, simulation)	30.27 ± 0.07	52.85 ± 0.08	27.85 ± 0.05
Young's modulus (E) (GPa)	0.07	0.36	0.43

[a] Reference 56. [b] Reference 58.

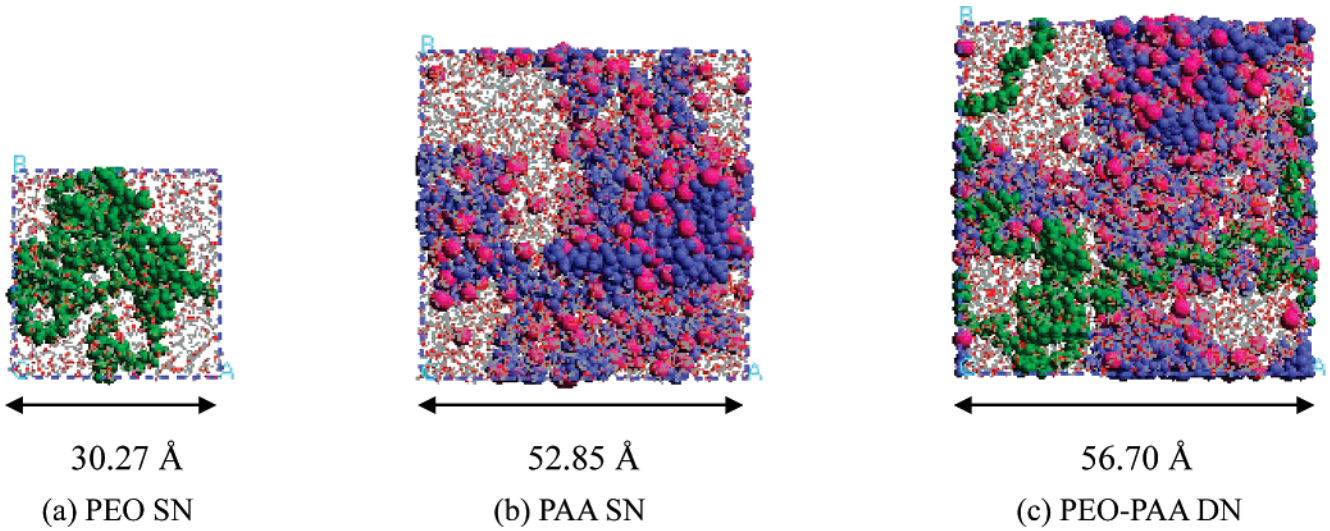

Figure 3. Equilibrated hydrogels. The PEO SN is green, and the PAA SN is blue. The Na^+ ions are pink balls.

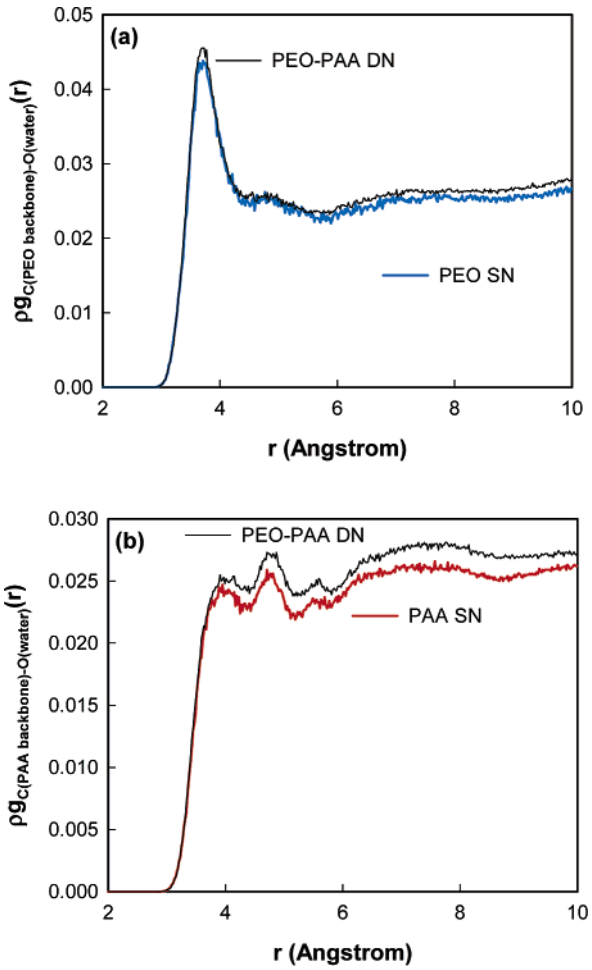

Figure 4. (a) Pair correlation function of carbon in the PEO backbone with the O of the water molecules. (b) Pair correlation function of carbon in the PAA backbone with the O of the water molecules. ρ is the number density of water in the hydrogel.

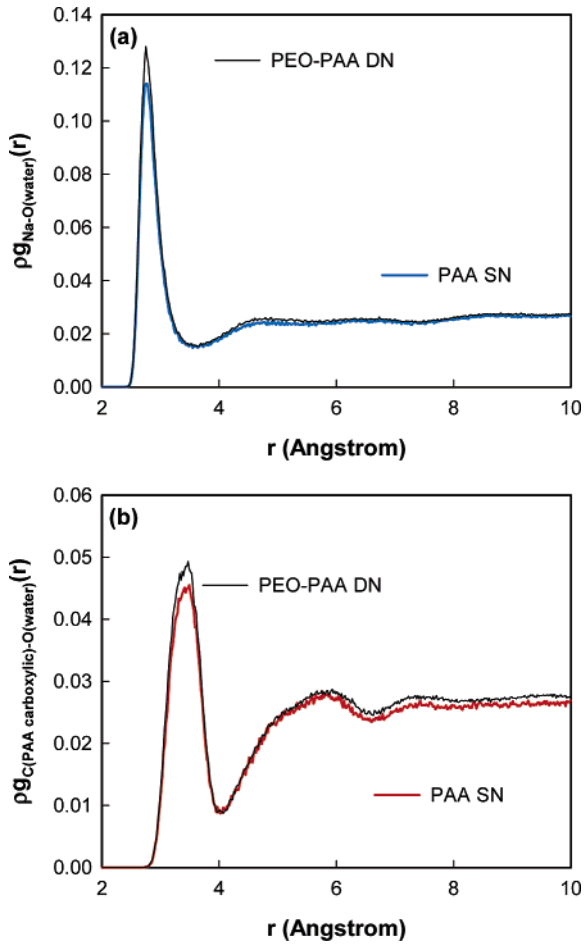

Figure 5. (a) Pair correlation function of Na^+ and the O of each water. Integrating over the first peak gives 5.5 for the PAA SN and 6.0 for the PEO−PAA DN. (b) Pair correlation function of the carboxylic carbon in PAA and the O of each water molecule. Integrating over the first peak gives 4.7 for the PAA SN and 5.1 for the PEO−PAA DN. ρ is the number density of water in the hydrogel.

For water, we used the F3C force field.[40] Thus, the force field has the following form:

$$E_{\text{total}} = E_{\text{vdW}} + E_Q + E_{\text{bond}} + E_{\text{angle}} + E_{\text{torsion}} + E_{\text{inversion}} \quad (1)$$

where E_{total}, E_{vdW}, E_Q, E_{bond}, E_{angle}, E_{torsion}, and $E_{\text{inversion}}$ are the total energies and the van der Waals, electrostatic, bond stretching, angle bending, torsion, and inversion components, respectively, and the force field parameters are described in the original papers.[32,40]

All of the MD simulations were performed using the MD code LAMMPS (large-scale atomic/molecular massively parallel simulator) from Plimpton at Sandia.[41,42] The equations of motion

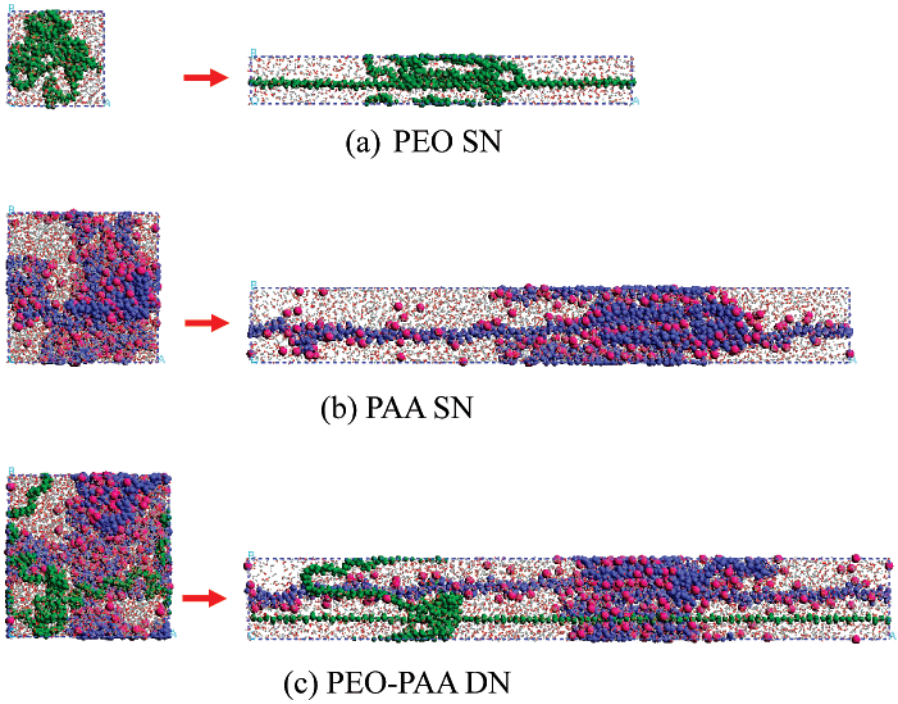

Figure 6. Uniaxial extension of hydrogels up to 300% strain. The size of all of the hydrogels is displayed in the same scale for direct comparison.

were integrated using the velocity-Verlet algorithm[43] with a time step of 1.0 fs. The Nose−Hoover temperature thermostat for the NVT and NPT MD simulations was used with a damping relaxation time of 0.1 ps and a dimensionless cell mass factor of 1.0. The atomic charges of the polymers were assigned using the charge equilibration (QEq)[44] method, and the atomic charges of the water molecules were from the F3C water model.[40] The particle−particle particle−mesh (PPPM) method[45] was used to calculate the electrostatic interactions.

2.2. Models and Simulations. All simulations were carried out using a full atomistic model. To prepare initial structures of the PEO−PAA DN hydrogel system, we first built homopolymers of PEO with a degree of polymerization (DP) of 30 for PAA with a DP of 80. To form a three-dimensional network structure, we put cross-linkers (acrylates) at both ends of the PEO polymer chain, to form the PEO−diacrylate (PEO−DA) macromer (Figure 1c), or one cross-linker (triethylene glycol dimethyacrylate (TEGDMA)) at one end of the PAA chain to form the PAA−TEGDMA macromer (Figure 1d).

As shown in Figure 2a, the next step is to build the SN structure of each polymer. Although experimental samples will always have structural variations such as free dangling chain ends and self-looping, we assumed a perfect network structure for both SN structures. Thus, through the periodic boundary conditions, all chains of the system participate in forming the network structure, leaving no free tangling chain ends or self-loops. In this perfect network structure, six chain ends meet together at a cross-linking point. After building the SN of each polymer, we put both SNs into the same simulation box to make a DN system (Figure 2b).

In the final stage, we added 5000 water molecules into the PEO−PAA DN system and replaced all of the hydrogen atoms of carboxylic acids in PAA with ionized Na atoms to form the salt. For doing this, we first prepared the conformationally extended DN system (Figure 2b) and the water box consisting of 5000 water molecules (0.087 g/cm^3) separately but with the same dimensions of 120 × 120 × 120 Å^3 and then integrated them into one simulation box. All close contacts of waters with polymer chains were resolved by simultaneous energy minimization (constant volume). After building and minimizing these hydrogel systems, we lead the systems to get contracted through 400 ps of NPT MD simulations at 300 K and 1 atm. Consequently, the water content of our PEO−PAA DN hydrogel is ∼76 wt %. As the reference systems for comparison, we built two independent SN hydrogels for PEO and PAA polymers with the same water content of 76 wt %. Table 1 summarizes the composition of DN and SN hydrogel systems.

After building these hydrogel systems, we equilibrated them through 400 ps of NVT MD simulations (to relax all contacts at the same density) followed by 600 ps of NPT MD simulations (to achieve the fully relaxed network systems). After finishing the building and equilibration steps described above, we ran 1.2 ns NPT MD simulations for data collection. All data reported in this paper were obtained from two independent samples using different initial configurations to provide the statistical uncertainties.

3. Results and Discussion

3.1. Equilibrated Structures. From our 1.2 ns NPT MD simulations, we obtained the average density of each hydrogel system (Table 1), they are 1.026 ± 0.006 g/cm^3 for the PEO SN, 1.160 ± 0.004 g/cm^3 for the PAA SN, and 1.136 ± 0.003 g/cm^3 for the PEO−PAA DN. The snapshots in Figure 3 show the final equilibrated structures of three hydrogel systems from the simulations, showing how hydrophilic polymer chains are mixed together with a vast amount of water (∼76 wt %).

Solvation of a Polymer Segment. An interesting point is that the PEO chain conformations in the DN hydrogel (Figure 3c) are expanded much more than that in the SN (Figure 3a). These differences in the conformational state are due to the cross-linking of the chains into a network structure. In other words, the PEO chains in the SN with dimensions of ∼30 Å must expand to be accommodated in the PEO−PAA DN with a larger dimension (∼56 Å). Such chain expansion eventually increases the chain solvation through increasing the water accessible area of the PEO chain. We expect that the PAA chains also undergo similar increases due to solvation, although the chain expansion is not as substantial as the PEO.

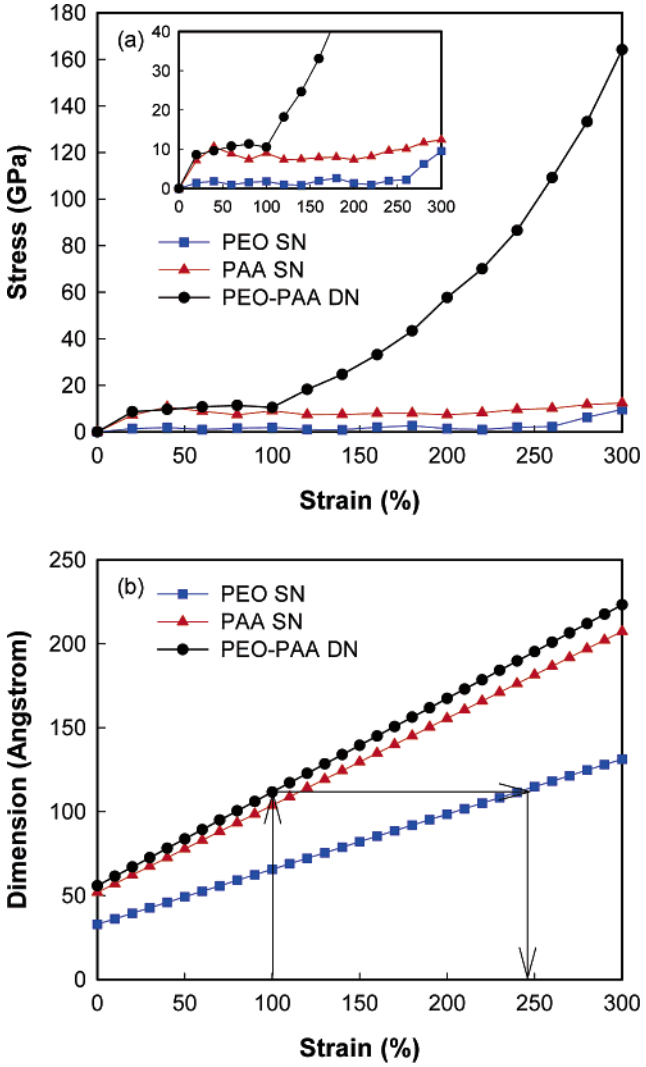

Figure 7. (a) Stress−strain curves of hydrogels. (b) Change of dimension as a function of strain. We observed that the stress in the DN increases rapidly from ∼100% strain, which corresponds to ∼250% strain for the PEO SN. The initial structure of the DN has ∼80% strain in the PEO part and ∼5% in the PAA.

To confirm this explanation, we analyzed the pair correlation function. The pair correlation function, $g_{A-B}(r)$, indicates the probability density of finding A and B atoms at a distance of r, averaged over the equilibrium trajectory as in eq 2

$$g_{A-B}(r) = \left(\frac{n_B}{4\pi r^2 dr}\right)/\left(\frac{N_B}{V}\right) \quad (2)$$

where n_B is the number of B particles located at the distance r in a shell of thickness dr from particle A, N_B is the number of B particles in the system, and V is the total volume of the system. We calculated $g_{C(PEObackbone)-O(Water)}(r)$ for the carbon (PEO backbone)−oxygen (water) pair and $g_{C(PAAbackbone)-O(Water)}(r)$ for the carbon (PAA backbone)−oxygen (water) pair, as shown in Figure 4. Both pair correlation functions in Figure 4 show clearly that the overall intensity of the PEO−PAA DN hydrogel is higher than that for the corresponding SN hydrogel, meaning that the polymer segments in the DN hydrogel have more water neighbors.

This observation was also confirmed by using Connolly surface analysis sampling of the chain structures of the PEO SN, PAA SN, and PEO−PAA DN along the trajectory files of our MD simulations, and we eliminated the H_2O molecules and calculated the Connolly surfaces of the networks using the standard probe radius of 1.40 Å. This provides the water accessible area. The results are the following: the Connolly surface of PEO is 4541.8 ± 90.4 Å^2 for the SN hydrogel and 4721.3 ± 34.4 Å^2 for the DN hydrogel, an increase of 4.9%, and the Connolly surface of PAA is 13699.0 ± 33.9 Å^2 for the SN hydrogel and 13906.1 ± 19.9 Å^2 for the DN hydrogel, an increase of 1.5%.

Thus, the surface area of each network is increased by incorporating it into DN hydrogel, indicating that the polymer chains of PEO and PAA in the DN hydrogel are exposed to more water than in the individual SN hydrogels. This is consistent with our pair correlation analysis.

Solvation of Ionic Moieties. We are also interested in the solvation of ionic moieties in our hydrogels.

Figure 5b shows the pair correlation function for the carboxylic carbon of the PAA and oxygen (water) pair, $g_{C(PAAcarboxylic)-O(Water)}(r)$. Here, the integrated average coordination number over the first peak is 4.7 for the PAA SN hydrogel and 5.1 for the PEO−PAA DN hydrogel, an 8% increase. This is consistent with our results of a 1.5% increase in the solvation area for the PAA segments in going from the SN to the DN.

Figure 5a compares the pair correlation functions for the Na^+ and oxygen (water) pair, $g_{Na-O(Water)}(r)$, between the PAA SN hydrogel and the PEO−PAA DN hydrogel. Integrating over the first peak of $g_{Na-O(Water)}(r)$, we find that the average water coordination numbers of the Na^+ ions are 5.5 for the PAA SN hydrogel and 6.0 for the PEO−PAA DN hydrogel. Both values for the water coordination numbers of ions in the hydrogel systems are in the range of the values in bulk water (5.4−6.0),[46−49] indicating that Na^+ solvation inside the hydrogel (with ∼76 wt % water content) is very close to that in bulk water. This observation of a 9% larger value for the water coordination of sodium in the DN hydrogel is also consistent with our results of a 1.5% increase in the solvation area for the PAA segments in going from the SN to the DN.

3.2. Characteristics of the Cross-Linked Network. The cross-linked network structure is the most distinct feature of hydrogel because such cross-linking, particularly chemical cross-linking, imparts high mechanical properties to the hydrogel system.[50−53] This network structure can be characterized in terms of M_c, the averaged molecular weight between cross-linking points, and ξ, the average mesh size defining the linear distance between consecutive cross-linking points.

These two parameters are known to have the following relationship:[20,22,54−56]

$$\xi = \upsilon_{2,s}^{-1/3}\left(C_n \frac{xM_c}{M_r} l^2\right)^{1/2} \quad (3)$$

where $\upsilon_{2,s}$ is the volume fraction of polymer in the swollen state, C_n is the characteristic ratio of the monomeric unit, M_r is the molecular weight of the monomeric unit, l is the segmental length of the monomeric unit, and x is a network topology coefficient ($x = 1.5$ for the ideal trifunctional network, $x = 2$ for the ideal tetrafunctional network, and $x = 3$ for the ideal hexafunctional network). The physical concept of eq 3 is to scale a Gaussian chain dimension between cross-linking points by the volume fraction to take account of its swollen state. Although eq 3 assumes the unperturbed Gaussian chain statistics that might not be achievable inside hydrogels,[50,57] this equation has been used in this field[20,54−56] to characterize the network structure of hydrogels synthesized under some controlled conditions.

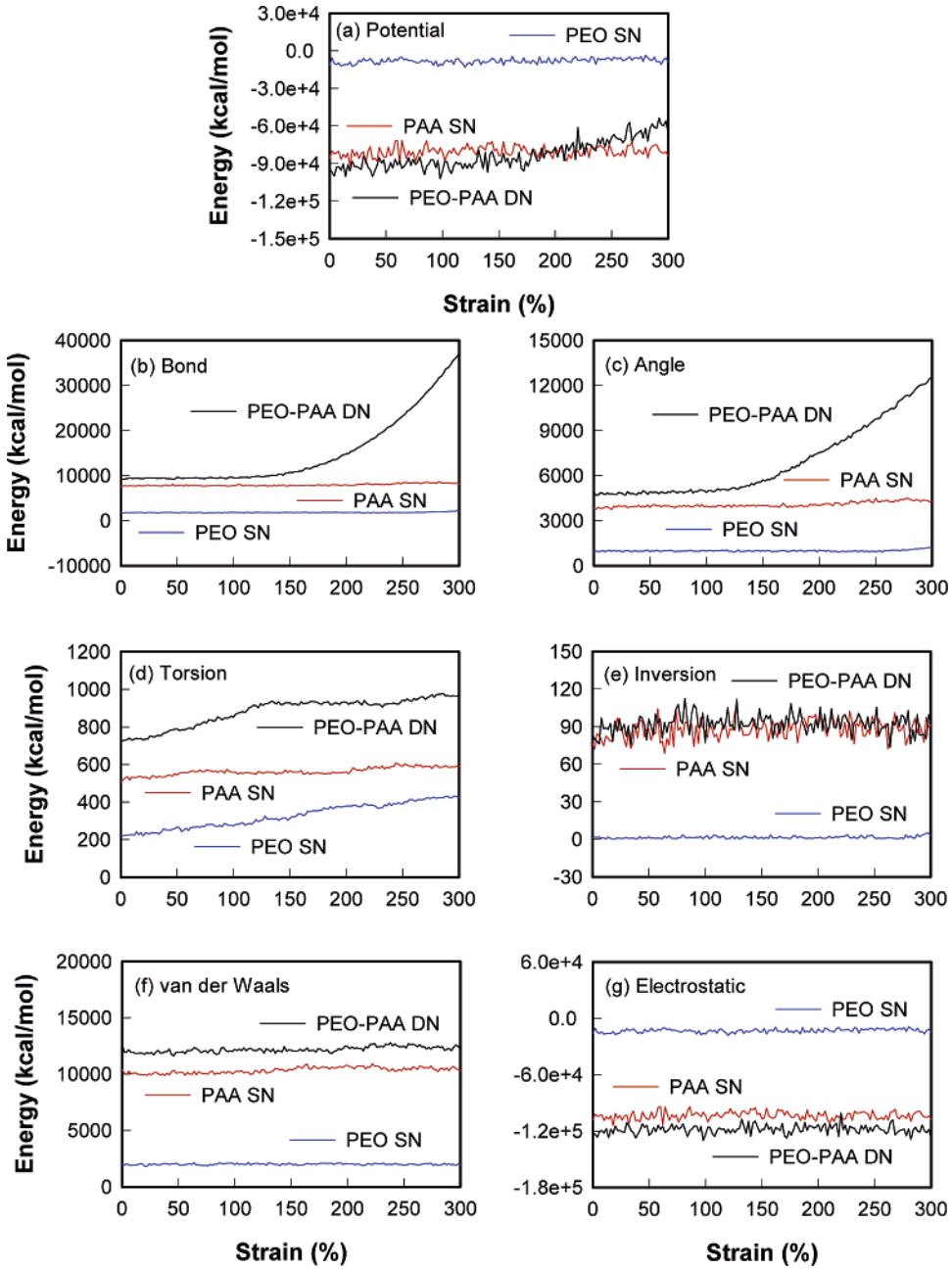

Figure 8. Changes of energy components as a function of strain.

We can test the assumptions in eq 3, since we can obtain the value of ξ directly from our simulations. According to the definition of ξ, the value of ξ of the SN hydrogel should be equal to the linear dimensions of the simulation box in our study, since our SN hydrogel systems are ideal hexafunctional networks with one cross-linking point in each simulation box (Figures 2 and 3). As summarized in Table 1, the mesh size of two SN hydrogels measured from our simulations is $\xi = 30.27 \pm 0.07$ Å for the PEO SN and $\xi = 52.85 \pm 0.08$ Å for the PAA SN. In contrast, the mesh size calculated from eq 3 is $\xi = 149.26$ Å for the PEO SN and $\xi = 220.36$ Å for the PAA SN, which shows an even larger mesh size than the simulated system. We think this overestimation is due to the unperturbed Gaussian chain assumption in eq 3.

On the other hand, the PEO−PAA DN hydrogel has two cross-linking points, leading to an effective mesh size of the DN hydrogel just half the mesh size of component networks, as summarized in Table 1 ($\xi = 27.85 \pm 0.05$ Å for the PEO−PAA DN). This will be useful in understanding the characteristics of the DN hydrogel system, as discussed in the following sections.

3.3. Mechanical Properties. *Stress−Strain Relationship.* To assess the mechanical properties of the hydrogels, we deformed the hydrogel systems uniaxially (*x*-axis direction) up to 300% of strain over a period of 600 ps. This was done continuously by applying a strain of 5×10^{-4}% every simulation step (1 fs) uniformly to the simulation box, and simultaneously, all atom coordinates were scaled to the new box. The stress (σ_{xx}) was calculated using the virial in eq 4.

$$\sigma_{xx} = \frac{1}{V}\sum_{i=1}^{N-1}\sum_{j=i+1}^{N} \mathbf{r}_{x,ij}\mathbf{f}_{x,ij} \tag{4}$$

where V, $\mathbf{r}_{x,ij}$, and $\mathbf{f}_{x,ij}$ are the volume, the position vector between atoms i and j (x component), and the force (x component) on atom i. Since the hydrogel is a three-dimensionally cross-linked

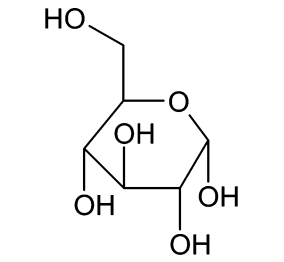

(a) D-glucose

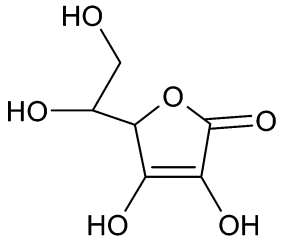

(b) Ascorbic acid

Figure 9. Model solute molecules for diffusion study in hydrogels.

network structure, we retained a constant volume while extending the deformation in one direction, by reducing the dimension in the other two directions such that the Poisson ratio was 0.5. These calculations were done at a constant temperature of 300 K.

Figure 6 shows the full change over the 600 ps, where we see that the conformation of the polymer chain in the deformation direction (*x*-axis) becomes extended while in the *y* and *z* directions the conformations become folded with reducing dimensions.

The stress−strain curves from our uniaxial extension simulation are presented in Figure 7a which is in good qualitative agreement with the experimental observations.[8,12,13] Thus, the stress of the DN hydrogel becomes much larger than the sum of the stresses of the two SN hydrogels after a certain strain (∼100% in this study). In order to understand the mechanical characteristics of the DN hydrogel, we analyzed the stress−strain curve by portioning the whole strain regime into two subregimes: one is a regime with a strain of ≤100% (regime A), and the other is a regime with a strain of >100% (regime B).

A feature of regime A is that the stress−strain response of the DN hydrogel is almost the same as a linear sum of those stress−strain responses from the two SN hydrogels. This means that, up to a strain of 100%, the two-component networks deform independently within their cross-linked structure without significant interaction between these two networks. For example, we can compare the Young modulus (E) as a representative elastic property of these hydrogels (calculated from the initial slope of the stress−strain curves in Figure 7a). As summarized in Table 1, we calculate that the Young modulus of the PEO−PAA DN hydrogel ($E_{PEO-PAA} = 0.43$ GPa) is equal to the sum of two SN hydrogels ($E_{PEO} = 0.07$ GPa for the PEO SN hydrogel and $E_{PAA} = 0.36$ GPa for the PAA SN hydrogel). Since the elastic response of material is at small deformation without permanent structural change, the result that

$$E_{PEO-PAA} \cong E_{PEO} + E_{PAA}$$

is clear evidence confirming that the two-component networks have no interference with each other when they are deformed in this regime A.

In contrast, regime B with a strain of >100% shows very different behavior: the stress of the PEO−PAA DN hydrogel

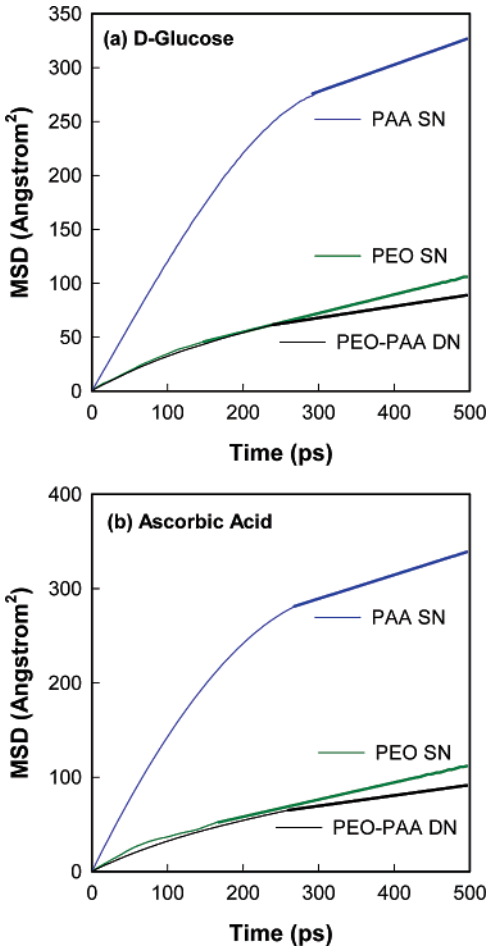

Figure 10. Mean-square displacement as a function of time of solute in the hydrogels at 300 K.

increases very rapidly as a function of strain. We interpret this as indicating that the cross-linking becomes effective in this regime. From Figure 7a, we observe the stress in the PEO−PAA DN hydrogel increases significantly after ∼100% of strain (at ∼111 Å of its physical dimension). To interpret the DN properties in region B, note that the initial unstrained DN has 80% strain in the PEO component and 5% strain in the PAA component. Thus, ∼100% strain in the DN corresponds to ∼250% strain in the PEO component and ∼16% strain in the PAA component. From Figure 7a, we see that ∼250% in the PEO SN is exactly where the stress in the PEO SN starts increasing dramatically.

From Figure 8, we see that the big contribution to the stress in the PEO SN above ∼250% is the angle strain. This indicates that the PEO is nearly fully extended and that further strain is affecting the internal valence energetics. Thus, incorporating the PEO SN into the PEO−PAA DN prestresses the DN so that 100% strain in the DN is equivalent to ∼250% stain in the PEO SN, the point at which it becomes quite stiff. Thus, the smaller M_c value of the PEO compared to the PAA is responsible for such high stress development in the DN hydrogel after 100% strain because the fully stretched conformation is reached much earlier than for the case of PAA with a larger M_c value. Our explanation seems consistent with the recent experimental observation by Gong and his co-workers.[8,13]

Energetics. Next, we analyze how the energies of hydrogels change with increased strain. Figure 8b−g shows the decomposition of the total potential energy (Figure 8a) into the components introduced in eq 1. The potential energies of the two SN hydrogels do not undergo a significant change with

TABLE 2: Concentration and Diffusion Coefficient of Solute

	PEO SN		PAA SN		PEO−PAA DN	
	D-glucose	ascorbic acid	D-glucose	ascorbic acid	D-glucose	ascorbic acid
number of molecules	1	1	5	5	6	6
concentration ($\times 10^{-2}$ M)	4.7	4.7	6.0	6.0	5.8	5.8
solute diffusion coefficient ($\times 10^{-5}$ cm^2/s)	0.173 ± 0.050	0.182 ± 0.045	0.249 ± 0.042	0.253 ± 0.046	0.107 ± 0.037	0.111 ± 0.034

	D-glucose	ascorbic acid
hydrodynamic radius (r_h) (Å)	2.78 ± 0.02	2.71 ± 0.03

increasing strain, whereas that of the PEO−PAA DN hydrogel increases gradually after 100% strain. Through the theory of rubber elasticity[50−53] dealing with the network structure (no solvent), it is understood that the stress built up during the deformation is due to conformational entropy, meaning that the change of energy is not a strong function of strain in the cross-linked network structure. As seen in Figure 8b−g, all of the energy components of the two SN hydrogels except the torsion energy (Figure 8d) seem to be insensitive to the strain up to nearly 300% strain. Indeed, the torsion angle is the most relevant factor for polymer conformation, so that the slight increase of torsion energy with increasing strain implies an entropic-driven stress behavior of the network structure. Therefore, we consider that the properties of these two SN hydrogels are consistent with the theory of rubber elasticity.

On the other hand, the PEO−PAA DN hydrogel shows a significant increase of its bond stretching energy and angle bending energy with increasing strain, especially after 150% strain. It seems obvious that these two energy components are responsible for the substantial stress development shown in Figure 7a because the PEO chain with a smaller M_c value in the DN hydrogel reaches its full extension earlier than the PAA chain, as explained in the previous section.

From these results, we could confirm that the improved mechanical strength of the DN hydrogel is due to the use of two SNs whose molecular weights (M_c) are different from each other and the component with a smaller M_c value takes a dominant role for this improvement. We also confirm that it is possible to impart such desirable mechanical performance to the DN hydrogel by controlling the molecular weight of the component SN.

3.4. Transport Properties. Solute molecule transport is another interesting aspect of hydrogel because of its applicability for biomedical and pharmaceutical technology. From numerous studies[15−19,55,56,58,59] focusing on the variables affecting the solute transport, it is understood that the transport is a function of such factors as mesh size, swelling ratio, ionization, ionic strength, pH condition, and temperature. In this section, we present our simulations for the diffusion of two small solute molecules: D-glucose and ascorbic acid (vitamin C).

To this end, first, we prepared initial structures by inserting the solute molecules (D-glucose and ascorbic acid, as shown in Figure 9) into the given equilibrated hydrogel systems and equilibrated these structures with 400 ps NPT MD simulations. The number of solute molecules was chosen so that there would be a similar concentration for all hydrogel systems. To obtain the mean-square displacement (MSD) of solutes in the hydrogels, we ran NPT MD simulations for 1 ns and calculated the diffusion coefficients (D) using

$$\langle (r(t) - r(0))^2 \rangle = 6Dt \tag{5}$$

using the linear part of the MSD in Figure 10. A simulation time of 1 ns may not be long enough to achieve accurate diffusion coefficients. The best test for a sufficient simulation time can be provided by a log−log plot of eq 5, where eq 5 leads to a value of 1.0 for the slope of this log−log plot. The results for our systems are shown in the Supporting Information, where we see that the slope is 0.74−0.82.

Table 2 shows that the diffusion coefficients of D-glucose and ascorbic acid are ~40% higher in the PAA SN hydrogel than in the PEO SN hydrogel. We assume that this is due to the ξ value of the PAA SN being ~75% higher than those of PEO. We do not know of experimental values to compare directly with our calculated diffusion coefficients, but our values are in the comparable range of other solutes: urea (0.89×10^{-5} cm^2/s), vitamin B_{12} (0.36×10^{-5} cm^2/s), dextran (0.089×10^{-5} cm^2/s), myoglobin (0.0016×10^{-5} cm^2/s), and theophylline (0.60×10^{-5} cm^2/s).[55,56,58]

For the PEO−PAA DN hydrogel, we find diffusion coefficients for both solutes that are only 40% of the value in the PAA SN, and even smaller than those for the PEO SN hydrogel (60%). We attributed this to the topological characteristics of the DN hydrogel having the smallest mesh size (27.85 Å) among the hydrogels (30.27 Å for the PEO SN hydrogel and 52.85 Å for the PAA SN hydrogel). Such a mesh-size dependency of diffusion has been observed in experiments using the hydrogels consisting of poly(vinyl alcohol) and poly(acrylic acid).[55,58,59]

Another point of interest is to compare the diffusion of the two different solutes under the same conditions. To assess the size of these solutes, we calculated their hydrodynamic radius ($\langle r_h \rangle$) using

$$\langle r_h \rangle^{-1} = \frac{1}{N^2} \sum_{j=2}^{N} \sum_{i=1}^{N} \left\langle \frac{1}{r_{ij}} \right\rangle \tag{6}$$

where N denotes the number of atoms in the solute molecule and r_{ij} is the distance between atoms i and j. The hydrodynamic radius of D-glucose is just 3% larger than that of ascorbic acid (2.78 ± 0.02 Å for D-glucose and 2.71 ± 0.03 Å for ascorbic acid, see Table 1), which we consider as insignificant for solute diffusion. Indeed, we found the same diffusion coefficients for ascorbic acid to be smaller than those for D-glucose by 5% for the PEO SN, 1.6% for the PAA SN, and 4% for the DN. Thus, the trend with hydrodynamic radius is the expected one, although it would have been interesting to consider solutes with bigger differences in their sizes.

4. Summary

Using atomistic NPT MD simulations, we prepared the DN hydrogel consisting of PEO and PAA with a molecular weight ratio of 1:5.4 (MW_{PEO}:MW_{PAA}) and a 76 wt % water content. For comparison, we also prepared the PEO and PAA SN hydrogels with the same molecular weight and water content as those used in the DN hydrogel.

Using criteria of the pair correlation function for the backbone carbon−water pair and of the solvent accessible surface area, we found that the polymers in the DN hydrogel have conformations that are expanded over the SN hydrogels. Thus, the

solvation by water is enhanced in the DN hydrogel by increasing the contact area with water molecules. Similarly, the carboxylate and sodium ionic moieties in the hydrogel are solvated more in the DN hydrogel than in the SN hydrogels.

We analyzed the mechanical properties of the hydrogels using uniaxial extension simulation in which the hydrogel system is extended up to 300% strain. We found that the stress−strain curves obtained from these simulations show that the DN hydrogel has a sudden increase of stress after ∼100% strain. Such a sudden increase in stress has been observed experimentally in DN hydrogels. We find that this sudden increase is due to the small value of M_c of the PEO, so that the PEO network reaches a fully stretched conformation by 100% strain in the DN, even though the PEO SN does not reach this point until 260% strain. We analyze the energy components to determine that the bond stretching energy and angle bending energy are responsible for this sudden increase of stress for the PEO−PAA DN hydrogel.

To investigate the transport properties of the DN hydrogel in comparison with the SN hydrogels, we inserted D-glucose and ascorbic acid solutes into the equilibrated hydrogels and calculated the diffusion coefficient for each solute using NPT MD simulations. We found that the diffusion coefficients of the solutes in the DN hydrogel are 60% of that in PEO SN and 40% of that in PAA SN, apparently because of the smaller mesh size.

Acknowledgment. The personnel in this project were partially supported with funding from NSF (CTS-0506951 and CTS-0608889). The facilities of the Materials and Process Simulation Center used for these studies were provided by DURIP-ARO, DURIP-ONR. M.Y.S.K. is a fellow of the Howard Hughes Medical Institute and the P&D Soros Foundation.

Supporting Information Available: Figures showing the diffusion of solutes in the SN or DN hydrogel and the convergence of energy in the equilibration procedure. This material is available free of charge via the Internet at http://pubs.acs.org.

References and Notes

(1) Harland, R. S., Prud'Homme, R. K., Eds. *Polyelectrolyte Gels: Properties, Preparation and Applications*; American Chemical Society: Washington, DC, 1992.
(2) Peppas, N. A. *Curr. Opin. Colloid Interface Sci.* **1997**, *2*, 531−537.
(3) Peppas, N. A.; Huang, Y.; Torres-Lugo, M.; Ward, J. H.; Zhang, J. *Annu. Rev. Biomed. Eng.* **2000**, *2*, 9−29.
(4) Lee, K. Y.; Mooney, D. J. *Chem. Rev.* **2001**, *101*, 1869−1879.
(5) Byrne, M. E.; Park, K.; Peppas, N. A. *Adv. Drug Delivery Rev.* **2002**, *54*, 149−161.
(6) Langer, R.; Peppas, N. A. *AIChE J.* **2003**, *49*, 2990−3006.
(7) Langer, R.; Tirrell, D. A. *Nature* **2004**, *428*, 487−492.
(8) Gong, J. P.; Katsuyama, Y.; Kurokawa, T.; Osada, Y. *Adv. Mater.* **2003**, *15*, 1155−1158.
(9) Farooqui, N.; Myung, D.; Masek, M.; Dalal, R.; Koh, W.; Gupta, S.; Noolandi, J.; Frank, C.; Ta, C. N. *Invest. Ophthalmol. Visual Sci.* **2005**, *46*, 873.
(10) Koh, W.-G.; Myung, D.; Ko, J.; Noolandi, J.; Frank, C. W.; Ta, C. N. *Invest. Ophthalmol. Visual Sci.* **2005**, *46*, 4994.
(11) Bakri, A.; Farooqui, N.; Myung, D.; Koh, W. G.; Noolandi, J.; Carrasco, M.; Frank, C.; Ta, C. N. *Invest. Ophthalmol. Visual Sci.* **2006**, *47*, 3592.
(12) Nakayama, A.; Kakugo, A.; Gong, J. P.; Osada, Y.; Takai, M.; Erata, T.; Kawano, S. *Adv. Funct. Mater.* **2004**, *14*, 1124−1128.
(13) Tanaka, Y.; Gong, J. P.; Osada, Y. *Prog. Polym. Sci.* **2005**, *30*, 1−9.
(14) Yasuda, K.; Gong, J. P.; Katsuyama, Y.; Nakayama, A.; Tanabe, Y.; Kondo, E.; Ueno, M.; Osada, Y. *Biomaterials* **2005**, *26*, 4468−4475.
(15) Kou, J. H.; Amidon, G. L.; Lee, P. I. *Pharm. Res.* **1988**, *5*, 592−597.
(16) Chou, L. Y.; Blanch, H. W.; Prausnitz, J. M.; Siegel, R. A. *J. Appl. Polym. Sci.* **1992**, *45*, 1411−1423.
(17) Hariharan, D.; Peppas, N. A. *J. Membr. Sci.* **1993**, *78*, 1−12.
(18) Ogawa, I.; Yamano, H.; Miyagawa, K. *J. Appl. Polym. Sci.* **1994**, *54*, 1971−1975.
(19) Khare, A. R.; Peppas, N. A. *Biomaterials* **1995**, *16*, 559−567.
(20) am Ende, M. T.; Hariharan, D.; Peppas, N. A. *React. Polym.* **1995**, *25*, 127−137.
(21) Bell, C. L.; Peppas, N. A. *Biomaterials* **1996**, *17*, 1203−1218.
(22) Flory, P. J.; Rehner, J. *J. Chem. Phys.* **1943**, *11*, 512−520.
(23) Flory, P. J.; Rehner, J. *J. Chem. Phys.* **1943**, *11*, 521−526.
(24) Katchalsky, A.; Lifson, S.; Eisenberg, H. *J. Polym. Sci.* **1951**, *7*, 571−574.
(25) Katchalsky, A.; Lifson, S.; Mazur, J. *J. Polym. Sci.* **1953**, *11*, 409−423.
(26) Lifson, S.; Katchalsky, A. *J. Polym. Sci.* **1954**, *13*, 43−55.
(27) Oldiges, C.; Tonsing, T. *Phys. Chem. Chem. Phys.* **2000**, *2*, 5630−5639.
(28) Tonsing, T.; Oldiges, C. *Phys. Chem. Chem. Phys.* **2001**, *3*, 5542−5549.
(29) Oldiges, C.; Tonsing, T. *Phys. Chem. Chem. Phys.* **2002**, *4*, 1628−1636.
(30) Oldiges, C.; Wittler, K.; Tonsing, T.; Alijah, A. *J. Phys. Chem. A* **2002**, *106*, 7147−7154.
(31) Oldiges, C.; Tonsing, T.; Wittler, K. *Phys. Chem. Chem. Phys.* **2002**, *4*, 5135−5141.
(32) Mayo, S. L.; Olafson, B. D.; Goddard, W. A., III. *J. Phys. Chem.* **1990**, *94*, 8897−8909.
(33) Jang, S. S.; Molinero, V.; Cagin, T.; Goddard, W. A., III. *J. Phys. Chem. B* **2004**, *108*, 3149−3157.
(34) Jang, S. S.; Lin, S.-T.; Cagin, T.; Molinero, V.; Goddard, W. A., III. *J. Phys. Chem. B* **2005**, *109*, 10154−10167.
(35) Jang, S. S.; Lin, S.-T.; Maiti, P. K.; Blanco, M.; Goddard, W. A., III; Shuler, P.; Tang, Y. *J. Phys. Chem. B* **2004**, *108*, 12130−12140.
(36) Jang, S. S.; Goddard, W. A., III. *J. Phys. Chem. B* **2006**, *110*, 7992−8001.
(37) Jang, S. S.; Jang, Y. H.; Kim, Y.-H.; Goddard, W. A., III; Flood, A. H.; Laursen, B. W.; Tseng, H.-R.; Stoddart, J. F.; Jeppesen, J. O.; Choi, J. W.; Steuerman, D. W.; DeIonno, E.; Heath, J. R. *J. Am. Chem. Soc.* **2005**, *127*, 1563−1575.
(38) Jang, Y. H.; Jang, S. S.; Goddard, W. A., III. *J. Am. Chem. Soc.* **2005**, *127*, 4959−4964.
(39) Jang, S. S.; Jang, Y. H.; Kim, Y.-H.; Goddard, W. A., III; Choi, J. W.; Heath, J. R.; Laursen, B. W.; Flood, A. H.; Stoddart, J. F.; Norgaard, K.; Bjornholm, T. *J. Am. Chem. Soc.* **2005**, *127*, 14804−14816.
(40) Levitt, M.; Hirshberg, M.; Sharon, R.; Laidig, K. E.; Daggett, V. *J. Phys. Chem. B* **1997**, *101*, 5051−5061.
(41) Plimpton, S. J. *J. Comput. Phys.* **1995**, *117*, 1−19.
(42) Plimpton, S. J.; Pollock, R.; Stevens, M. *The Eighth SIAM Conference on Parallel Processing for Scientific Computing*; Minneapolis, MN, 1997.
(43) Swope, W. C.; Andersen, H. C.; Berens, P. H.; Wilson, K. R. *J. Chem. Phys.* **1982**, *76*, 637−649.
(44) Rappe, A. K.; Goddard, W. A., III. *J. Phys. Chem.* **1991**, *95*, 3358−3363.
(45) Hockney, R. W.; Eastwood, J. W. *Computer Simulation Using Particles*; McGraw-Hill International Book Co.: New York, 1981.
(46) Clementi, E.; Barsotti, R. *Chem. Phys. Lett.* **1978**, *59*, 21−25.
(47) Mezei, M.; Beveridge, D. L. *J. Chem. Phys.* **1981**, *74*, 6902−6910.
(48) Chandrasekhar, J.; Spellmeyer, D. C.; Jorgensen, W. L. *J. Am. Chem. Soc.* **1984**, *106*, 903−910.
(49) Cieplak, P.; Kollman, P. *J. Chem. Phys.* **1990**, *92*, 6761−6767.
(50) Flory, P. J. *Principles of Polymer Chemistry*; Cornell University Press: Ithaca, NY, 1953.
(51) Treloar, L. R. G. *The Physics of Rubber Elasticity*, 3rd ed.; Clarendon Press: Oxford, U.K., 1975.
(52) Sperling, L. H. *Introduction to Physical Polymer Science*, 2nd ed.; John Wiley & Sons: New York, 1992.
(53) Gedde, U. W. *Polymer Physics*, 1st ed.; Chapman & Hall: London, 1995.
(54) Gudeman, L. F.; Peppas, N. A. *J. Appl. Polym. Sci.* **1995**, *55*, 919−928.
(55) Peppas, N. A.; Wright, S. L. *Macromolecules* **1996**, *29*, 8798−8804.
(56) Russell, R. J.; Axel, A. C.; Shields, K. L.; Pishko, M. V. *Polymer* **2001**, *42*, 4893−4901.
(57) Flory, P. J. *Statistical Mechanics of Chain Molecules*; John Wiley & Sons: New York, 1969.
(58) Gudeman, L. F.; Peppas, N. A. *J. Membr. Sci.* **1995**, *107*, 239−248.
(59) Peppas, N. A.; Wright, S. L. *Eur. J. Pharm. Biopharm.* **1998**, *46*, 15−29.